JOURNAL OF APPLIED CRYSTALLOGRAPHY

Volume 53 (2020)

Supporting information for article:

Best Practices for Operando Depth-Resolving Battery Experiments

Hao Liu, Zhuo Li, Antonin Grenier, Gabrielle E. Kamm, Liang Yin, Gerard S. Mattei, Monty R. Cosby, Peter G. Khalifah, Peter J. Chupas and Karena W. Chapman

1. Derivation of geometrical aberrations associated with center of mass shifts

The major geometrical aberrations resulting from tilt misalignment of the samples are all related to changes in the sample center of mass. A rough schematic of the experiment geometry is shown below in Figure S1. During the experiment, the sample is translated up and down with respect to the static X-ray beam (black arrow). However, this behavior is mathematically equivalent to the beam moving up and down with respect to the sample, and the discussion will be framed in this alternate frame of reference. The heights reported in the main text of the manuscript are the "height normal to the beam" with respect to the sample center (black dot), and therefore reflect the coordinates with respect to the experiment (vertical axis of Figure S1) rather than the height normal to the circular faces of the samples. It should be noted that the while the aspect ratio of the rectangle in Figure S1 is about 3:1, that the aspect ratio of typical samples is usually closer to 20:1.

The cross-section of the sample illuminated by the beam during experiments is very nearly rectangular, despite the cylindrical nature of typical experiments done in a radial geometry (radial illumination of sample), and it will be assumed to be an ideal rectangle for derivations. When the sample is perfectly aligned, the path that the beam traverses through the sample will always be equal to the distance between the front and back of the sample as the height of the beam changes with respect to the sample center, and this length will be equal to the sample diameter if the beam is centered with respect to the horizontal profile of the sample. If the sample is slightly tilted, there will be regions (in gray) where the beam no longer enters and exits through the left and right sides of the rectangular cross-section of the sample, but instead passes through one side and one face (top or bottom) of the sample. For a tilted sample, the horizontal center of mass with respect to a given vertical position of the beam is the average of the entry and exit point coordinates. The center of mass for tilted samples is most easily calculated with respect to the corners, and it either consists of the corner point (**A** & **D** in Figure S1), or the midpoint (**B** & **C**) of the line between the corner and the opposite edge.

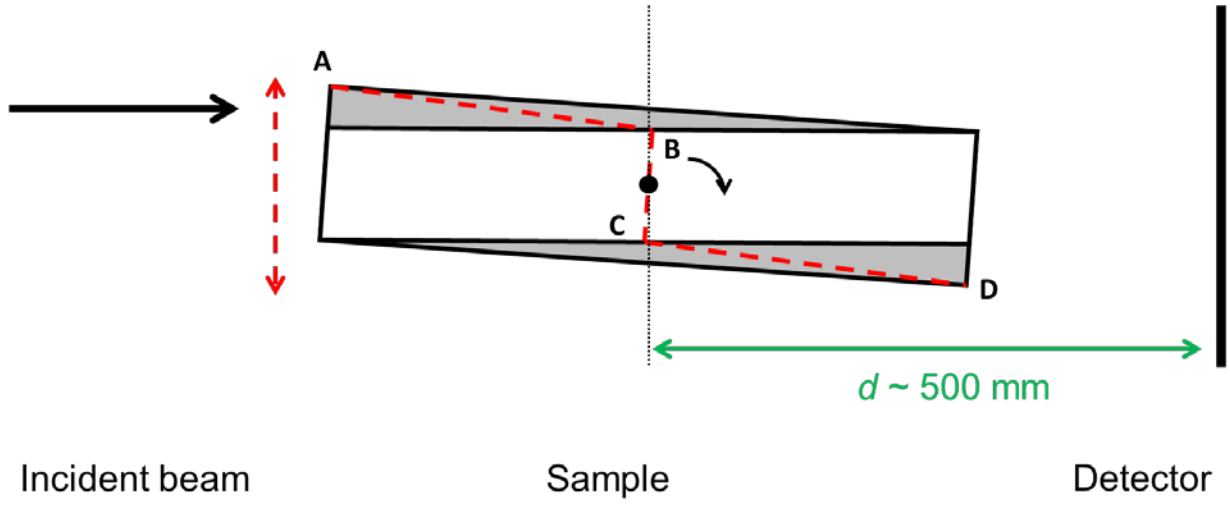

Figure S1. Schematic of experimental geometry for a typical depth profiling experiment in which the position of the incident beam (black arrow) is varied in the vertical direction with respect to the sample. The sample center of mass at different beam heights is indicated by a red dashed line.

For center of mass calculations, we choose to use the sample frame of reference rather than the beam frame of reference used in the main text. The coordinate system is shown below in Figure S2, where the horizontal axis is parallel to the long axis of the rectangular sample along which the length of the sample is measured, and the orthogonal vertical axis is parallel to the short axis of the sample along which the thickness of the sample is measured. The interior black lines indicate the path of X-rays passing through a sample corner and are necessarily parallel to each other since the synchrotron beam divergence is negligible with respect to the sample dimensions. The angle between these lines and the long edges of the sample is denoted θ and is equal to the tilt of the sample relative to the beam, thus specifying the sample misalignment. If the coordinates of the four points **A**, **B**, **C**, and **D** are calculated, the center of mass offset (in the sample coordinates) for any other incident beam vertical position can be calculated from the equation of the line segment connecting two of these points. It should be noted that the geometry of Figure S2 represents only one of the seven unique geometries that result from tilts of less than 90°, all of which are shown in Figure S3.

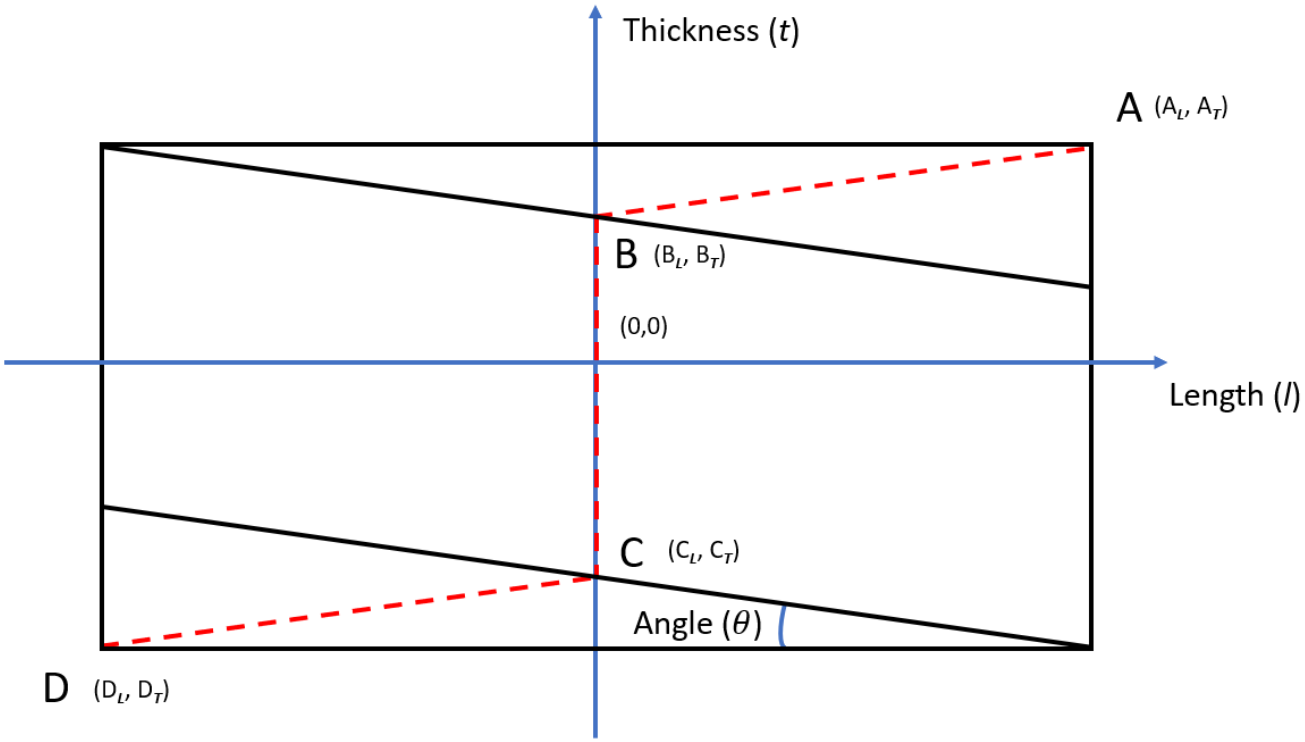

Figure S2. Sample frame of reference for calculating the center of mass for any beam path. The dashed red line denotes the center of mass positions for all possible incidence points of X-ray beams that are tilted with respect to the sample by an angle θ (as drawn here, the value of θ is positive) The path of the X-ray beam when it intersects corners of the sample while passing through the samples are drawn as the two black lines containing the points **B** or **C**. The points **A**, **B**, **C** and **D** are the end points of the three line segments which are used to calculate the center of mass for any specific incidence point of the X-ray beam.

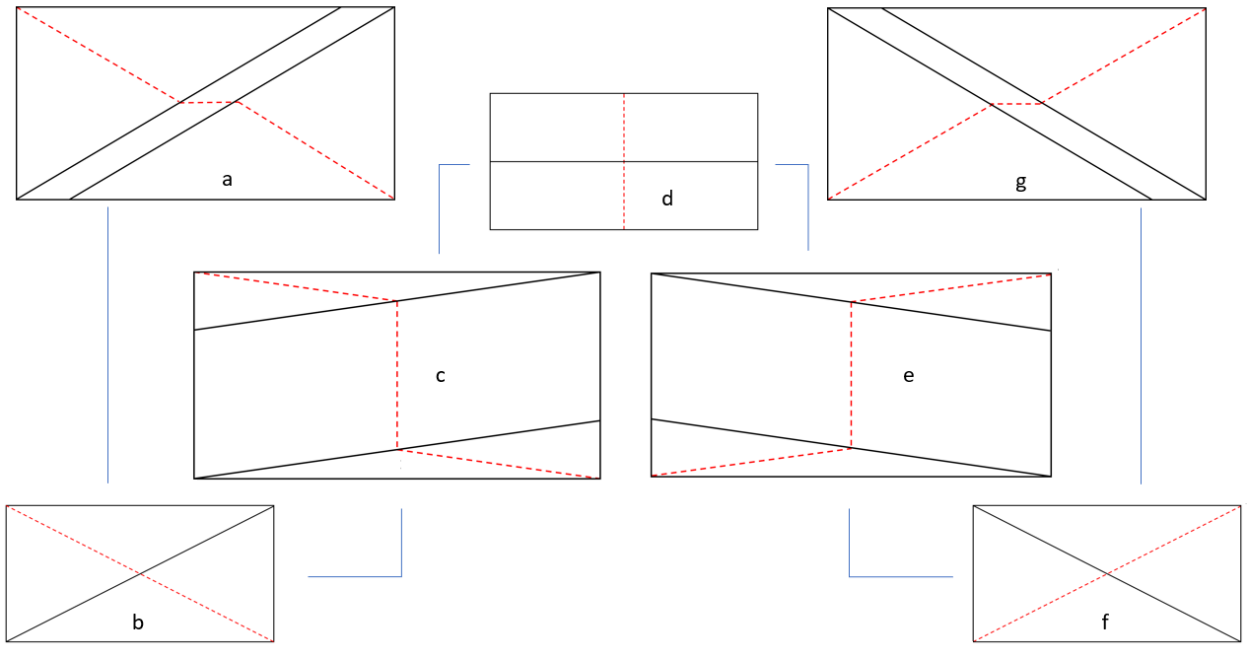

Figure S3. Seven possible geometries of intersection of X-ray beam with sample for tilts < 90° (labeled **a** – **f** in order of decreasing tilt angle, from most positive to most negative).

The coordinates (in the sample frame of reference) of the key points (**A**-**D**) needed for sample center of mass calculations are provided in Table S1. All equations for the line segments between pairs of consecutive points (again, in the sample frame of reference) are provided in Table S2, together with the boundary conditions which specify the limits of the line segments. The derivation of these equations is discussed further in the next section. The final step in calculations is to take the results obtained in this manner and transform them back in to the beam frame of reference, which involves rotation by an angle θ. A generic line specified by the equation $mx + b$ in the sample frame of reference will transform into an alternate line with the equation $m'x + b'$ in the beam frame of reference that is obtained using the standard transformations below:

$$m' = \frac{m\cos\theta - \sin\theta}{m\sin\theta + \cos\theta} \text{ and } b' = \frac{b}{m\sin\theta + \cos\theta}$$

Table S1. Horizontal and vertical coordinates for points **A-D** in the sample frame of reference for the seven different experiment geometries shown in Figure S3.

	A_t	A_l	B_t	B_l	C_t	C_l	D_t	D_l
a	$\frac{T}{2}$	$\frac{-L}{2}$	0	$\frac{T}{2}\cot\theta - \frac{L}{2}$	0	$\frac{L}{2} - \frac{T}{2}\cot\theta$	$\frac{-T}{2}$	$\frac{L}{2}$
b	$\frac{T}{2}$	$\frac{-L}{2}$	N/A	N/A	N/A	N/A	$\frac{-T}{2}$	$\frac{L}{2}$
c	$\frac{T}{2}$	$\frac{-L}{2}$	$\frac{T}{2} - \frac{L}{2}\tan\theta$	0	$\frac{L}{2}\tan\theta - \frac{T}{2}$	0	$\frac{-T}{2}$	$\frac{L}{2}$
d	$\frac{T}{2}$	0	N/A	N/A	N/A	N/A	$\frac{-T}{2}$	0
e	$\frac{T}{2}$	$\frac{L}{2}$	$\frac{T}{2} + \frac{L}{2}\tan\theta$	0	$-\frac{L}{2}\tan\theta - \frac{T}{2}$	0	$\frac{-T}{2}$	$\frac{-L}{2}$
f	$\frac{T}{2}$	$\frac{L}{2}$	N/A	N/A	N/A	N/A	$\frac{-T}{2}$	$\frac{-L}{2}$
g	$\frac{T}{2}$	$\frac{L}{2}$	0	$\frac{L}{2} + \frac{T}{2}\cot\theta$	0	$-\frac{T}{2}\cot\theta - \frac{L}{2}$	$\frac{-T}{2}$	$\frac{-L}{2}$

Table S2. Equations and boundary conditions for line segments describing the center of mass positions in the seven different experiment geometries shown in Figure S3.

	f(AB)	boundary	f(BC)	boundary	f(CD)	boundary
a	$l = -\cot\theta\, t - \frac{L}{2} + \frac{T}{2}\cot\theta$	$l \in \left[-\frac{L}{2}, \frac{T}{2}\cot\theta - \frac{L}{2}\right]$	$t = 0$	$l \in \left[\frac{T}{2}\cot\theta - \frac{L}{2}, \frac{L}{2} - \frac{T}{2}\cot\theta\right]$	$l = \cot\theta\, t + \frac{L}{2} - \frac{T}{2}\cot\theta$	$l \in \left[\frac{L}{2} - \frac{T}{2}\cot\theta, \frac{T}{2}\right]$
b	$l = -\cot\theta\, t$			$t \in \left[\frac{-T}{2}, \frac{T}{2}\right]$		
c	$l = -\cot\theta\, t - \frac{L}{2} + \frac{T}{2}\cot\theta$	$t \in \left[\frac{T}{2} - \frac{L}{2}\tan\theta, \frac{T}{2}\right]$	$l = 0$	$t \in \left[\frac{L}{2}\tan\theta - \frac{T}{2}, \frac{T}{2} - \frac{L}{2}\tan\theta\right]$	$l = \cot\theta\, t + \frac{L}{2} - \frac{T}{2}\cot\theta$	$t \in \left[\frac{-T}{2}, \frac{L}{2}\tan\theta - \frac{T}{2}\right]$
d	$l = 0$			$t \in \left[\frac{-T}{2}, \frac{T}{2}\right]$		
e	$l = -\cot\theta\, t - \frac{L}{2} - \frac{T}{2}\cot\theta$	$t \in \left[\frac{T}{2} + \frac{L}{2}\tan\theta, \frac{T}{2}\right]$	$l = 0$	$t \in \left[-\frac{L}{2}\tan\theta - \frac{T}{2}, \frac{T}{2} + \frac{L}{2}\tan\theta\right]$	$l = \cot\theta\, t + \frac{L}{2} + \frac{T}{2}\cot\theta$	$t \in \left[\frac{-T}{2}, -\frac{L}{2}\tan\theta - \frac{T}{2}\right]$
f	$l = -\cot\theta\, t$			$t \in \left[\frac{-T}{2}, \frac{T}{2}\right]$		
g	$l = -\cot\theta\, t - \frac{L}{2} - \frac{T}{2}\cot\theta$	$l \in \left[\frac{L}{2} + \frac{T}{2}\cot\theta, \frac{L}{2}\right]$	$t = 0$	$l \in \left[-\frac{T}{2}\cot\theta - \frac{L}{2}, \frac{L}{2} + \frac{T}{2}\cot\theta\right]$	$l = \cot\theta\, t + \frac{L}{2} + \frac{T}{2}\cot\theta$	$l \in \left[\frac{-L}{2}, -\frac{T}{2}\cot\theta - \frac{L}{2}\right]$

2. Derivation of equations for lines used in center of mass calculations

As shown in Figure S2, the cross-section of the sample probed by the X-ray beam during experiments is reasonably approximated by a rectangle with a length L and width T. Additionally, the angle θ is defined as the angle between the incident beam and the bottom of the sample using the coordinate system described in Figure S2, where a positive value of θ indicates that a clockwise rotation of the sample (when viewed from the perspective of Figure S2) is required to co-align the sample with the beam.

To determine the center of mass of the sample in the horizontal direction when the beam does not pass through the sample center (a key step in determining the effective horizontal distance offset relative to the distance to the sample center), the first step is to determine which of the three regions of the sample the beam is probing. As shown in Figure S2, one of these regimes is typically an interior region of the sample where the distance displacement is minimal and the horizontal center of mass falls on the line **BC**. The other two regions are typically exterior regions where the displacements can be comparable in magnitude to the half-width of the sample, where the sample center of mass falls on lines **AB** or on **CD**. For special cases where the beam is exactly parallel to the sample edge (case **d** in Figure S3) or where the tilt angle is such that the beam can pass through two corners as it transits the sample (cases **b** and **f** in Figure S3), there are fewer than 3 mathematically distinct regions, as can be seen in Tables S1 and S2.

In all cases, the horizontal center of mass for the beam passing through the sample for a given vertical displacement relative to the sample center within the sample frame of reference is found by determining the intersection point of the beam with the lines (**AB**, **BC**, and **CD**) that describe the possible center of mass positions for the beam intersecting the tilted sample. The coordinates (*l*, *t*) of the four points that determine this line (**A**, **B**, **C** and **D**) along the orthogonal axis in the direction of the sample length and thickness are given as a function of the tilt angle (θ), the total sample length (L), and the total sample height (T) in Table S1, and can be derived through simple geometric relationships. Furthermore, the equations for the line and the boundary conditions that produce the line segments **AB**, **BC**, and **CD** are given in Table S2.

3. Derivation of common crossing points for distance displacements at different tilt angles

In Figure 5 of the main text, it was shown that the unknown length and thickness of a sample cross-section can be determined from plots of the crossing points of the plots of the displacement distance *vs.* relative beam height for different sample tilt angles. These special crossing points occur at coordinates corresponding to 1/2 of the sample length and 1/4 of the sample thickness when the tilt angle is small.

This relationship between the coordinates of these special crossing points and the sample dimensions can be mathematically proved by carrying out the calculation for the sample horizontal center of mass at two different tilt angles, θ and φ, and solving these equations to determine when common coordinates (*l*,*t*) are produced on a given line segment (such as AB) as shown below:

(1) $$l = \cot\theta t + \frac{L}{2} - \frac{T}{2}\cot\theta$$

(2) $$l = \cot\varphi t + \frac{L}{2} - \frac{T}{2}\cot\varphi$$

(3) $$l = \cot 2\theta t + \frac{L\sin\theta - T\cos\theta}{2\sin 2\theta}$$

(4) $$l = \cot 2\varphi t + \frac{L\sin\varphi - T\cos\varphi}{2\sin 2\varphi}$$

Equations (1) and (2) give coordinates on the line segment **AB** at different tilt angles of θ and φ, respectively, with regard to the sample coordinate system. However, these equations can't be

directly used for comparisons of experimental data collected at different tilt angles since the coordinates *l* and *t* since the sample axes have a different orientation for different tilt angles. To remedy this, the equations can both be transformed to the beam frame of reference as described earlier in Section 1 of the Supporting information, resulting in equations (3) and (4).

Once this is done, the equations for *l* can be used to derive the following equality:

(5) $$\cot 2\theta t + \frac{L\sin\theta - T\cos\theta}{2\sin 2\theta} = \cot 2\varphi t + \frac{L\sin\varphi - T\cos\varphi}{2\sin 2\varphi}$$

The crossing point coordinate *t* can be found by rearranging Equation (5) to solve for *t*:

(6) $$t = \frac{L(\sin\theta\sin 2\varphi - \sin\varphi\sin 2\theta) + T(\cos\varphi\sin 2\theta - \cos\theta\sin 2\varphi)}{2(\cos 2\theta\sin 2\varphi - \cos 2\varphi\sin 2\theta)}$$

Since θ and φ are both small angles ($< 5°$), $\cos\varphi \cong \cos\theta \cong \cos 2\theta \cong 1$ and Equation (6) can thus be simplified as:

(7) $$t = \frac{L(\sin\theta\sin 2\varphi - \sin\varphi\sin 2\theta)}{2(\sin 2\varphi - \sin 2\theta)} - \frac{T}{2}$$

Since $\frac{L(\sin\theta\sin 2\varphi - \sin\varphi\sin 2\theta)}{2(\sin 2\varphi - \sin 2\theta)} \ll \frac{T}{2}$ the first part of Equation (7) can be ignored and $t \cong -\frac{T}{2}$

The corresponding value of *l* can be found at $t = -\frac{T}{2}$:

(8) $$l = \cot 2\theta \times (-\frac{T}{2}) + \frac{L\sin\theta - T\cos\theta}{2\sin 2\theta}$$

Which can be rewritten as:

(9) $$l = \frac{L\sin\theta}{2\sin 2\theta} - \frac{T\cos\theta + T\cos 2\theta}{2\sin 2\theta}$$

At low angles, $\sin\theta \cong \theta$ where θ is the angle in units of radians, allowing (9) to be simplified:

(10) $$l = \frac{L}{4} - \frac{T\cos\theta + T\cos 2\theta}{2\sin 2\theta}$$

Since $\frac{T\cos\theta + T\cos 2\theta}{2\sin 2\theta} \ll \frac{L}{4}$ the second part of Equation (10) can be ignored and $l \cong \frac{L}{4}$

Thus at low angles, the two crossing points will occur at values of $(\frac{T}{2}, \frac{L}{4})$ and $(\frac{-T}{2}, \frac{-L}{4})$ in the beam frame of reference. This relationship can be utilized to experimentally determine the length and thickness of the sample in the beam during experiments by collecting vertical scans across each angle in a small tilt series (e.g., 0°, 0.5°, 1.0°, 1.5°, 2.0°). As such, it offers a simple contactless diffraction method for determining the thickness of cathode films with micron-scale precision.

4. Influence of sample distance errors on apparent lattice parameters

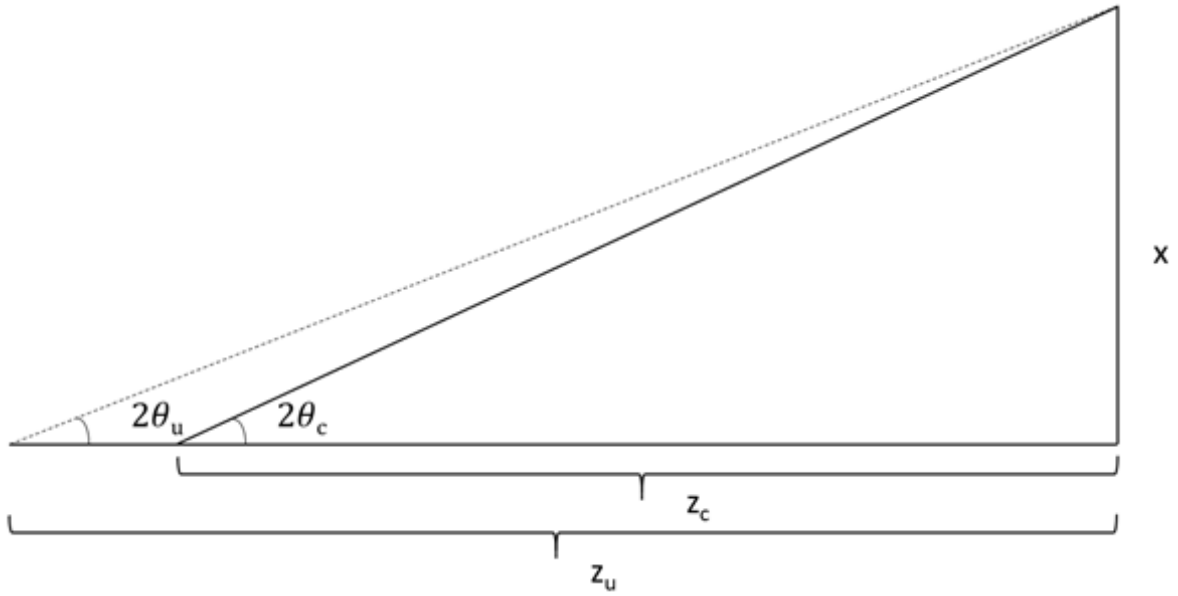

Figure S4. Schematic representation of the influence of sample center of mass displacements on the experimental determination of diffraction angles and lattice parameters. Here, *x* is the radial distance from the beam center to a diffraction ring on a 2D area detector and *z* is the sample-to-detector distance. The correct (or true) distance or angle is labelled with a subscript *c* while the uncorrected (or apparent) distance or angle is labelled with a subscript *u*.

If corrections for the sample center of mass displacement are not implemented during the step of data integration, the refined lattice parameters will have errors that are approximately proportional to the error in the sample-to-detector distance, as seen in the derivation below. To a first approximation, these errors can be corrected by linearly rescaling the lattice parameter data so that the lattice parameters are correct at a reference point in time (*e.g.*, scale to match the known lattice parameters of the pristine material on diffraction data collected before the start of battery cycling). However, since the correction is only approximately linear (with the deviation increasing at higher diffraction angles), such corrections are only appropriate for preliminary data analyses.

For data collected on a misaligned (tilted) sample at a specific beam height relative to the sample center, if the uncorrected assumed sample-to-detector distance (z_u) is used for integration instead of the true distance (z_c) that properly corrects for sample center of mass shifts, then the uncorrected *d*-spacing for a given reflection (d_u) will approximately differ from the true *d*-spacing for the reflection (d_c) through the relationship: $d_u = d_c\ (z_u / z_c)$, as seen in the derivation below:

(11) $$\lambda = 2\mathrm{d}\sin\theta$$

(12) $$\left(\frac{d_u}{d_c}\right)^2 = \left(\frac{2\lambda/\sin\theta_u}{2\lambda/\sin\theta_c}\right)^2 = \left(\frac{\sin\theta_c}{\sin\theta_u}\right)^2$$

At low angles, $\sin\theta \approx \theta$ where θ is the angle in units of radians, thus:

(13) $$2sin\theta = 2\theta = sin2\theta$$

By combining (12) and (13):

(14) $$\left(\frac{d_u}{d_c}\right)^2 = \left(\frac{\sin\theta_c}{\sin\theta_u}\right)^2 = \left(\frac{\frac{1}{2}\sin 2\theta_c}{\frac{1}{2}\sin 2\theta_u}\right)^2 = \left(\frac{\sin 2\theta_c}{\sin 2\theta_u}\right)^2 = \frac{\frac{x^2}{x^2+{z_c}^2}}{\frac{x^2}{x^2+{z_u}^2}} = \frac{x^2+{z_u}^2}{x^2+{z_c}^2}$$

In a typical diffraction experiment, ${x^2} \ll {z_c}^2$ so $\left(\frac{d_u}{d_c}\right)^2 \approx \frac{{z_u}^2}{{z_c}^2}$ and thus:

(15) $$d_u = \frac{d_c \times z_u}{z_c}$$

Due to this relationship, a 1% error in detector will distance produce an error of about 1% in each of the three cell lattice parameters and of about 3% error in the unit cell volume. To verify this result, data reduction was conducted for a series of sample-to-detector distances (952 mm, 951 mm, 950 mm, 949 mm, 948 mm, and 947 mm) that deviate from the actual value (953 mm) for the same diffraction pattern of a $LiNi_{0.8}Co_{0.15}Al_{0.05}O_2$ sample. This deliberate variation in the sample-to-detector distance for data reduction simulates the scenario where the sample-to-detector distance varies within the sample. In agreement with (15), the relative change in the d-spacing of a Bragg reflection scales with the relative deviation from the actual sample-to-detector distance (Figure S5). Some simulated volume changes that illustrate the effect of detector distance and sample tilt on the error magnitude are given in Figure S6.

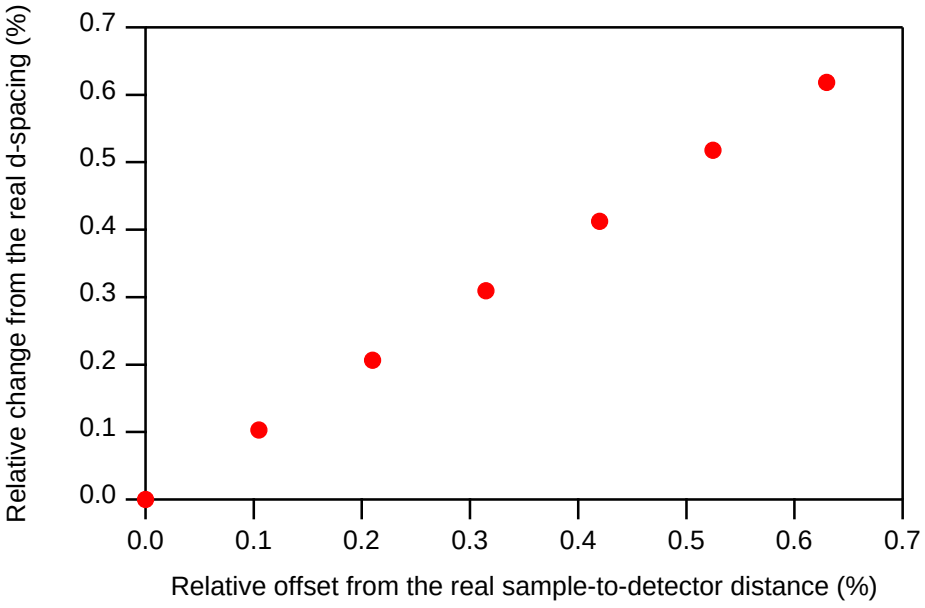

Figure S5. Relative change in the apparent d-spacing for the (113) reflection of a $LiNi_{0.8}Co_{0.15}Al_{0.05}O_2$ sample when the 1D diffraction pattern is reduced from the same 2D diffraction image for various sample-to-detector distances.

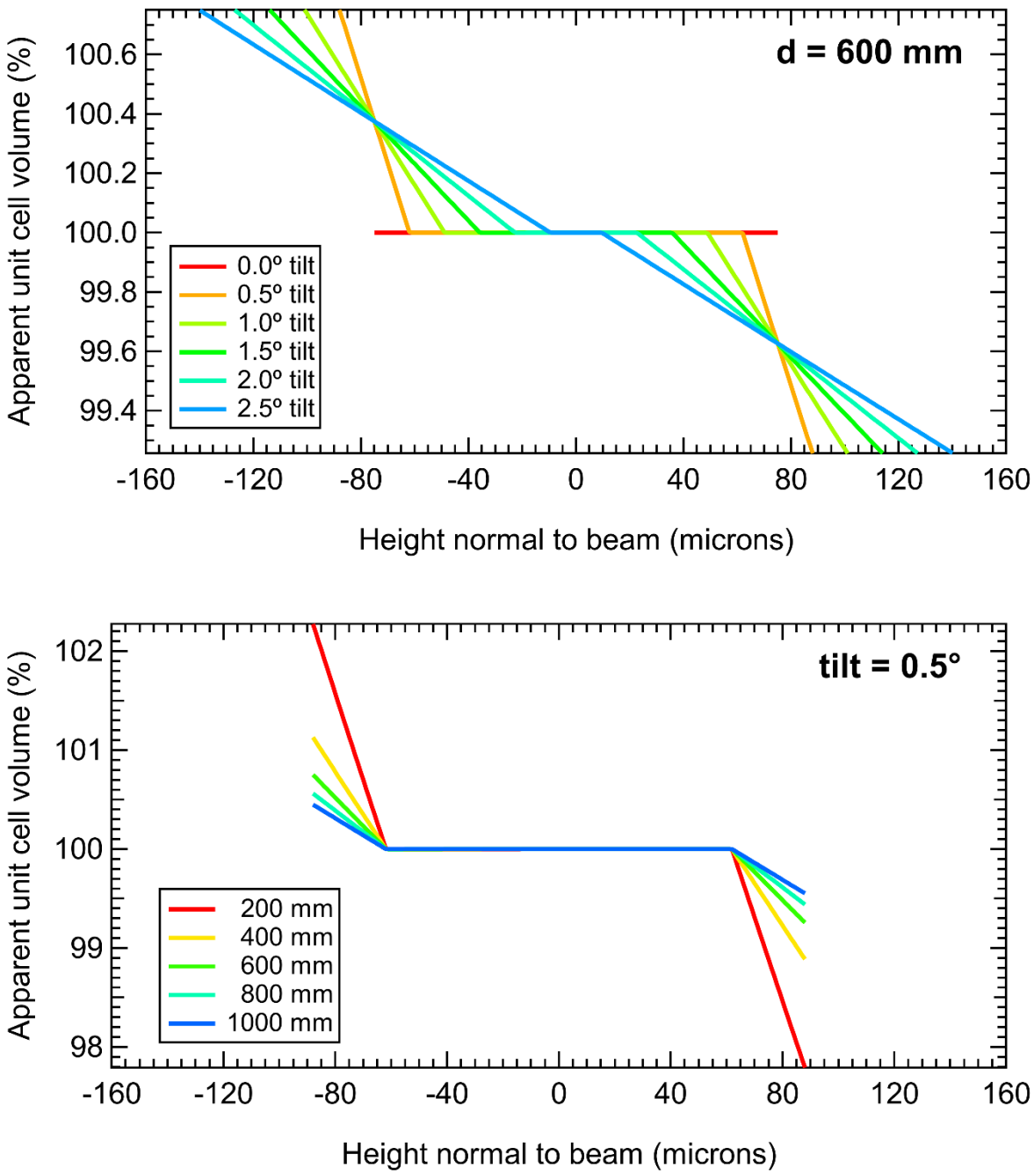

Figure S6. Simulated volume changes for a NMC811 sample that result from variable changes in the tilt angle at a fixed detector distance of 600 mm (top) or from variable changes in the detector distance at a fixed tilt angle (bottom). The largest errors occur near the edge of the sample while errors near the sample center are negligible (top) and that the error magnitude is inversely proportional to the detector distance (bottom).